

# LED-based near infrared sensor for cancer diagnostics

Andrey Bogomolov<sup>\*a, b</sup>, Vladimir Ageev<sup>a</sup>, Urszula Zabarylo<sup>a, c</sup>, Iskander Usenov<sup>a, d</sup>,  
Franziska Schulte<sup>a</sup>, Dmitry Kirsanov<sup>e</sup>, Valeria Belikova<sup>b</sup>, Olaf Minet<sup>c</sup>, E. Feliksberger<sup>f</sup>,  
I. Meshkovsky<sup>f</sup>, Viacheslav Artyushenko<sup>a</sup>

<sup>a</sup>art photonics GmbH, Rudower Chaussee 46, 12489 Berlin, Germany;

<sup>b</sup>Samara State Technical University, Molodogvardeyskaya 244, 443100 Samara, Russia;

<sup>c</sup>Dept. of Medical Physics and Optical Diagnostics, Charité Universitätsmedizin Berlin, Fabeckstraße  
60-62, 14195 Berlin, Germany;

<sup>d</sup>Dept. of Optics and Atomic Physics, Technical University of Berlin, Straße des 17. Juni 135,  
10623 Berlin, Germany;

<sup>e</sup>Institute of Chemistry, St. Petersburg State University, Universitetskaya nab. 7/9, St. Petersburg,  
Russia

<sup>f</sup>St. Petersburg National Research University of Information Technologies, Mechanics and Optics,  
49 Kronverksky Pr., St. Petersburg, 197101, Russia

## ABSTRACT

Optical spectroscopic technologies are increasingly used for cancer diagnostics. Feasibility of differentiation between malignant and healthy samples of human kidney using Fluorescence, Raman, MIR and NIR spectroscopy has been recently reported<sup>1</sup>. In the present work, a simplification of NIR spectroscopy method has been studied. Traditional high-resolution NIR spectrometry was replaced by an optical sensor based on a set of light-emitting diodes at selected wavelengths as light sources and a photodiode. Two prototypes of the sensor have been developed and tested using 14 *in-vitro* samples of seven kidney tumor patients. Statistical evaluation of results using principal component analysis and partial least-squares discriminant analysis has been performed. Despite only partial discrimination between tumor and healthy tissue achieved by the presented new technique, the results evidence benefits of LED-based near-infrared sensing used for oncological diagnostics.

**Keywords:** cancer diagnostics, optical sensor, near infrared, sensor, LED

## 1. INTRODUCTION

478.000 new cases of cancer were diagnosed in 2012 only in Germany. A rising number of incidences is recorded every year. As an early detection of the disease improves the survival rate drastically, enhanced screening methods are needed. Therefore, the demand for easy-to-handle cheap instruments is high. Cancer diagnostics is necessary to develop a proper treatment strategy. Currently, cancer is diagnosed through a variety of techniques. There are non-invasive (ultrasound, X-rays, CT scans, etc.) and invasive (diagnostic surgery, including a biopsy) procedures. In the clinical praxis there are also a few blood tests, which detect cancer-related antigens, but these are far from being definitive. Methods using optical spectroscopy are well equipped to enable fast and reliable measurements of a high number of patients. Additionally, these techniques are non-invasive and can be used *in-vivo* offering results without time delay and during routine checkups.

Diagnostics in general consist of tests performed to determine the presence of cancer, to characterize its histological structure and to determine the degree of its advancement. It is of great importance to diagnose cancer at an early stage before it has got a chance to grow and to spread. Cancer cells can spread from their origin to other parts of the body, where they can grow into new tumors. Such secondary tumors or metastases are more difficult to treat, and generally, patient's survival chances are reduced.

Since the early 1990s, several clinical groups have used spectroscopic methods to distinguish between normal and neoplastic tissues. Today, spectroscopic methods in tumor diagnostics are called spectral histopathology. With optical methods it is possible to detect pathological and morphological changes non-invasive and without Xeno-markers. Whereas,

\*abo@artphotonics.com; phone 49 30 6779 887-0; fax 49 30 6779 887-99; artphotonics.com

using well-known markers such as NADH and FADH only invasive diagnostics is possible. Detailed knowledge of the changes in chemical composition correlated to pathological cell and tissue functions will affect the development of all new diagnostic procedures and therapeutic approaches. Optical methods open up new possibilities for the "next generation" of spectral pathology applications. Recent studies<sup>1</sup> show that malignant and healthy tissues may be differentiated by fluorescence or molecular spectroscopy methods: Raman scattering, IR-absorption or diffuse reflection (Fig. 1). One of the most promising optical methods is near-infrared (NIR) spectroscopy. It is useful for disease diagnosis because of its potential to probe the changes of tissue at the molecular level. This method can rapidly capture information about chemical bonds in functional groups and is, therefore, sensitive to changes in molecular composition and structure.

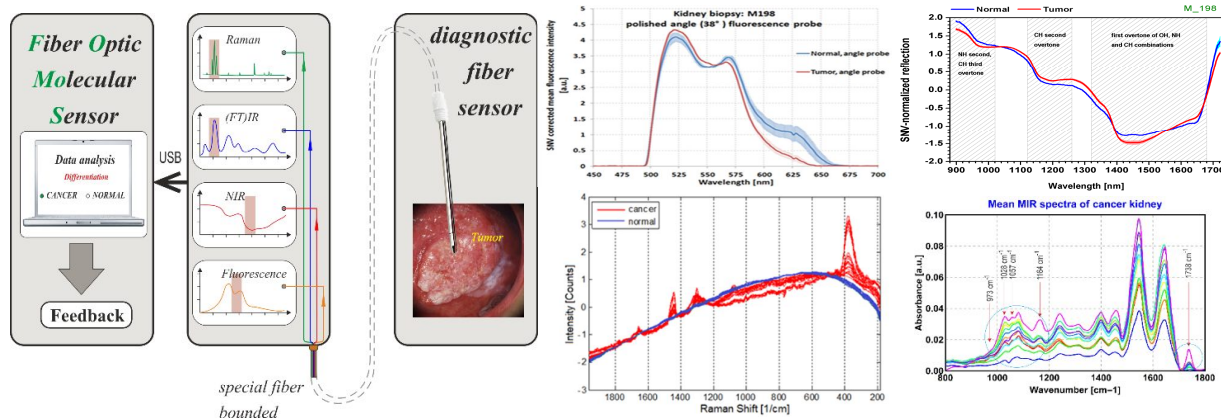


Fig1. Multi Spectral Fiber (MFS) tissue analyzer (left); Fluorescence, NIR DOS, Raman and MIR ATR spectra of cancer and normal tissue of kidney.

NIR diffuse reflection optical spectroscopy as an adjunct diagnostic modality to image-guided needle biopsy presents enormous potential for increasing feasibility and effectiveness of cancer detection. Percutaneous, image-guided core needle biopsy is less invasive, less expensive and faster than conventional surgical biopsy. It minimizes deformity, leaves little or no scarring and requires a short time for tissue recovery. NIR spectroscopy established at the tip of a needle was able to successfully differentiate malignant tumor from benign tissue by targeted performance<sup>2</sup>. NIR spectroscopic analysis was as well successfully used to distinguish between cancer tissue and normal tissue of liver<sup>3</sup>, breast<sup>4,5,6,7</sup>, cervix<sup>8</sup>, oral cancer<sup>9,10,11</sup>, prostate<sup>12,13</sup>, lung<sup>14</sup>, gastric<sup>15</sup> and esophagus<sup>16</sup>.

Due to a relatively high penetration depth up to 2-3 mm<sup>17,18</sup>, non-invasiveness and high speed of analysis, NIR spectroscopy is one of the most promising tools for cancer diagnostics. It can be easily combined with fiber cables and probes, adding a flexibility that is necessary under clinical conditions, e.g. during a surgical intervention.

Recent studies in various application fields have shown that full-scale NIR spectroscopy can be replaced by optical sensor measurements at several specific wavelengths optimized for a specific application<sup>19,20,21,22</sup>.

This simplification is not necessarily associated with a loss in accuracy. In some cases, sensor performance can be as good as that of similar full-scale spectroscopic methods, or even better<sup>19</sup>. Some expected losses related to the much lower resolution of the sensor are compensated by the elimination of non- (or less) informative wavelengths from the analysis, such as noise or irrelevant variances. This also leads to the data and model simplification, and consequently, improves the reliability of the modeling (e.g. discrimination) results.

In the present study a novel tumor-sensing device based on light emitting diodes (LEDs) working in NIR region has been developed. Two prototypes of the sensor have been constructed and tested for kidney cancer detection using *in-vitro* clinical samples of seven patients.

## 2. MATERIALS AND METHODS

### 2.1 Samples

In this study, NIR spectral measurements were performed on unstained cryo biopsies of normal and tumor renal tissue in the Klinik für Urologie, Charité Universitätsmedizin Berlin (Germany). Samples were derived from 7 patients after

nephrectomy. The institutional ethics committee approved the sampling and further investigation of renal tissues (ethical approval: EA1/134/12). Histological classification was performed according to the World Health Organization (WHO) criteria. Grading was accomplished according to Fuhrman<sup>23</sup> and staging met the UICC criteria<sup>24</sup>. Prior to measurements, tissue samples were thawed for 5 minutes at room temperature.

In the first series of spectroscopic investigations with the first LED-sensor prototype (data set A), three pairs of biopsy samples (191, 194, and 198) were measured. All tumor samples in the first series were of grade 2. According to the Fuhrman nuclear grading system (FNG)<sup>25</sup>, grade 2 means slightly irregular contours and diameters of approximately 15 $\mu$ m with nucleoli visible at 400x.

In the next series of measurements with an improved sensor prototype (section 2.2), four pairs of renal biopsies (144, 149, 151 and 160) were investigated. Tumor samples in the second series were of grade 2, 1, 2 and 3 respectively. All tumor samples were of the predominant cCRCC (clear cell renal cell carcinoma) subtype. This experimental series is referred to as data set B.

Both, tumor and normal, tissue samples of renal biopsies were placed into small Petri dishes 35 mm in diameter. Samples were fixated to the Petri dishes with a small amount of tissue adhesive glue (TRUGLUE<sup>®</sup>) to avoid shifting of the tissue during measurement. On the outer surface of every Petri dish, a grid with numbered fields was drawn. The measurements were performed at each position which was completely covered by biopsy.

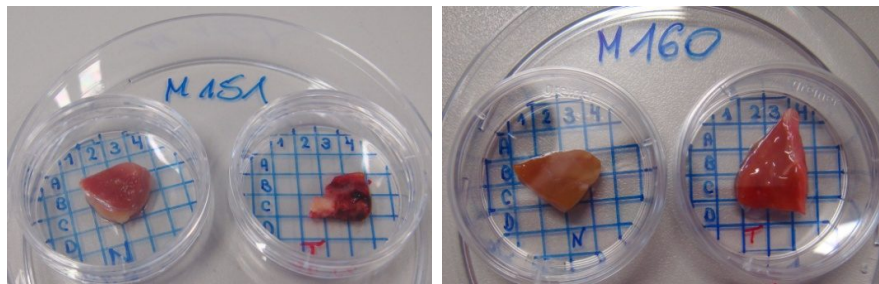


Fig. 2. Renal biopsies of patients 151 and 160 respectively: healthy (left) and tumor (right) tissue.

In the present text, individual data are coded in accordance with the sample type (“T” for tumor and “N” for normal tissue), patient number and spectral measurement number. In the data set B, an additional index like *C3*, *Cn* or *B2* denotes a specifically marked measurement position (see Fig. 2). For instance, *N144\_Cn\_5* denotes measurement #5 in the position *Cn* of the normal tissue sample of patient 144.

## 2.2 Sensor construction and data acquisition

The concept of a LED-sensor is based on rapid scanning of a few (typically, two to seven) selected wavelengths. The LEDs at the chosen wavelengths are used for an alternating illumination of the sample. The reflected light is then measured by photodiode.

In the present study, four wavelengths were selected: 0.94  $\mu$ m (channel 4), 1.17  $\mu$ m (channel 3), 1.30  $\mu$ m (channel 1) and 1.44  $\mu$ m (channel 2). The wavelengths near 1.0  $\mu$ m and 1.45  $\mu$ m were chosen to be close to the maxima of water absorption bands while the LED at 1.2  $\mu$ m mostly corresponds to the absorption of lipids<sup>26</sup>. The possibility to detect cancer using a water-to-lipid ratio in tissue with NIR spectroscopy was reported in<sup>27, 28</sup>. The third channel was intended as a scatter-correcting channel as it corresponds to a “low-populated” spectral region around 1.3  $\mu$ m.

The measurements were performed using a vertically mounted thin metal-coated probe (Fig. 3, right). In the first experiment (data set A) the probe end was in contact with the tissue samples through a thin (about 0.5 mm) quartz glass covering the sample. In the second experiment (data set B) with an improved sensor prototype the probe equipped with a sapphire window at the Brewster’s angle ( $\sim 60.5^\circ$ ) (Fig. 3, right), only the sharp-angled tip of the probe (and not the window itself) was in direct contact with the sample. Therefore, in the latter case, the measurement was performed at some distance from an uncovered probe surface.

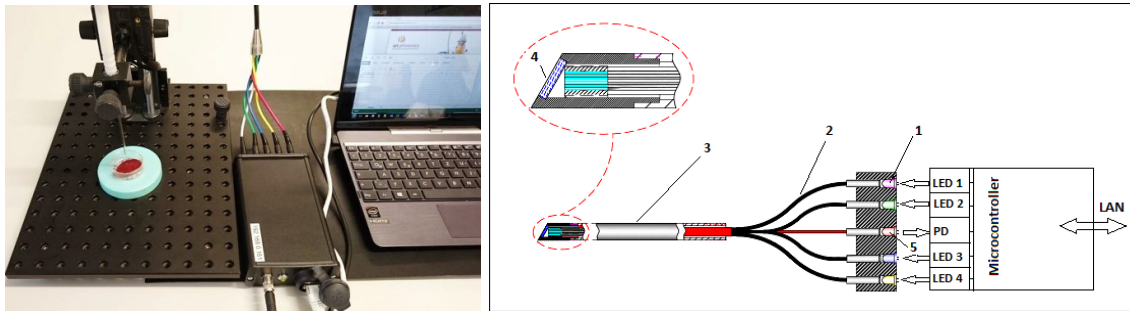


Fig. 3. Probe construction and measurement setup. (Left) experimental setup used for data acquisition in data set B; (right) probe construction schematic: 1 - LEDs, 2 - fiber cables, 3 - stainless steel tube, 4 - sapphire window (in data set A the probe tip had a right-angle shape and was not protected by a glass window).

The sensor voltage data (in mV) were recorded using a software written in LabView by National Instruments™ (USA).

### 2.3 Data analysis

Prior to the analysis, the data variables (individual channels) were mean centered. No further preprocessing was applied. One evident outlier (sensor measurement *NI94\_5*) has been removed from the data set A prior to analysis. Principle component analysis (PCA)<sup>29</sup> and partial least-squares discrimination analysis (PLS-DA)<sup>30</sup> were used for data analysis.

Data treatment and chemometrics analysis were performed in MATLAB R2008b (The MathWorks™ Inc., USA) supplemented with PLS\_Toolbox v.7.5 (Eigenvector Research Inc., USA) and in TPT cloud ([www.tptcloud.com](http://www.tptcloud.com)), a web-based chemometrics software by Global Modelling (Germany) and Samara State Technical University (Russia).

## 3. RESULTS AND CONCLUSIONS

The data sets A and B acquired using two respective sensor prototypes (section 2.2) are closely similar (Fig. 4). The mean signal curves (Fig. 4, bottom left and bottom right) have the same characteristic shape with a pronounced minimum at 1.44  $\mu\text{m}$  and the highest intensities observed at 1.30  $\mu\text{m}$ . The measurements of all sensor channels show an essential variance. The scatter of values is particularly high for the channels 1 and 4 (1.30 and 0.94  $\mu\text{m}$ ). Generally, lower data intensity in the case of data set B is accounted for another measurement geometry associated with some losses of the incident and re-emitted light, i.e. a larger distance to the sample and the presence of a relatively thick sapphire window located at an angle to the measurement surface (section 2.2). Some individual measurements in both data sets have different shapes.

As it is clearly seen from the mean signals (Fig. 4, bottom left and bottom right) the tumor tissues are basically characterized by a higher intensity of detected signal at all studied wavelengths. This is an evidence of higher light scattering by the tumor tissue.

Cancer cells have in comparison to normal cells larger nuclear-cytoplasmic ratios. They show nuclear enlargement, asymmetrical nuclear shape and increased DNA content. The differences observed by NIR DOS correspond to alterations related to the interaction between light and cells. Microscopically the tumor cells of cCRCC (clear cell renal cell carcinoma) are arranged in compact nests, sheets, alveolar, or acinar structures separated by thin-walled blood vessels. Tumor cells have clear cytoplasm. The diameter of non-cancer cell nuclei is typically 5-10  $\mu\text{m}$ , whereas cancer cell nuclei can be as large as 20  $\mu\text{m}$ . In this dense network of cells, probably nuclei are the most significant scatterers<sup>31</sup>. The spectrum of backscattered light contains a component that varies characteristically with wavelength, (with this variation) depending on particle size and refractive index.

Another evident data feature is a much lower variance of the measured sensor values in the case of healthy tissue samples. The simplest explanation of this fact is that normal kidney is more homogeneous in terms of cell structure than tissue affected by cancer. All clear cell RCCs have characteristic golden yellow appearance due to the rich lipid content of their cells. The cut surface is often very inhomogeneous with a varying degree of blood particles, necrosis, cystic degeneration and calcification<sup>32</sup>. Sometimes this difference can even be observed by the naked eye (Fig. 2).

The intensity of the backscattered light seems to be the main characteristic feature distinguishing normal and tumor tissue samples. Indeed, preliminary data analysis has shown that application of any scatter-correcting preprocessing technique, such as Standard Normal Variate or using the measurement at 1.3  $\mu\text{m}$  or another channel as an “internal” reference, is disadvantageous for the model discrimination power. Therefore, the modeling was performed by multivariate analysis of the raw data sets A and B.

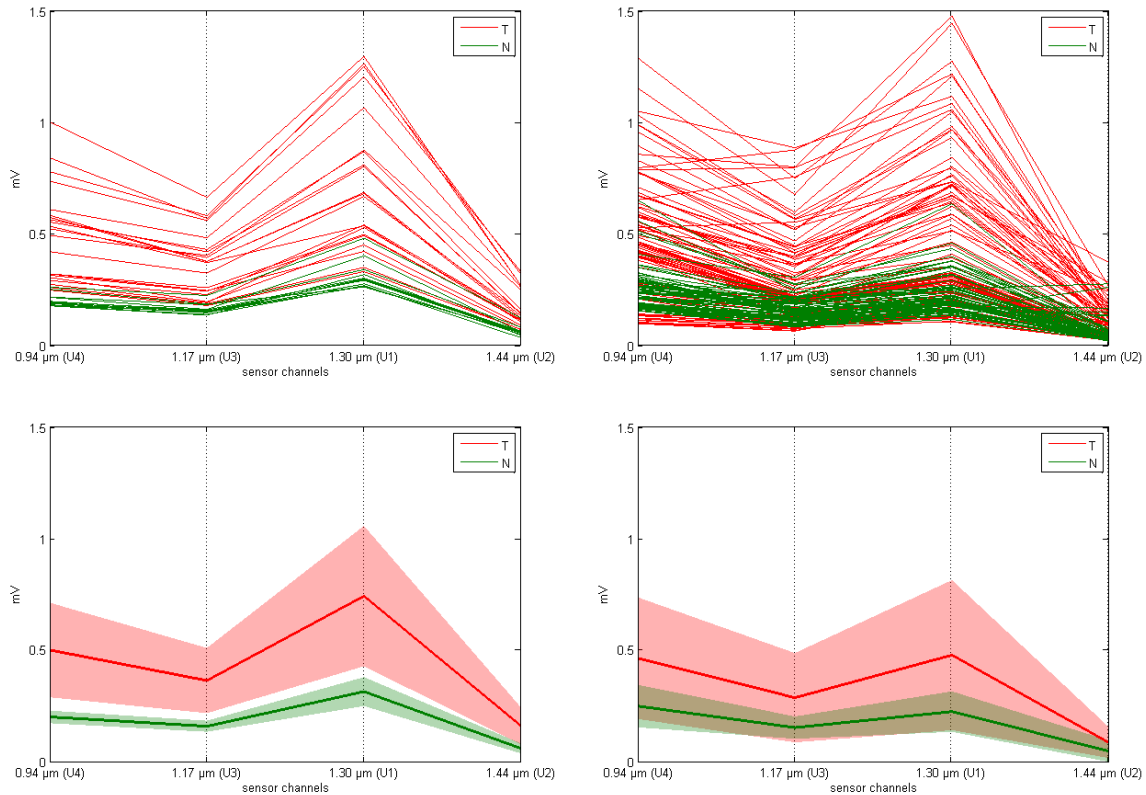


Fig. 4. Sensor data: (top left) data set A, (top right) data set B, (bottom left and right) data mean and standard deviation in data sets A and B, respectively.

PCA score plots (Fig. 5) are convenient to estimate the general quality of cancer discrimination in data sets A and B. In the data set A (Fig. 5, top) the tumor/normal class separation is almost complete. Cancer recognition in the plane of two first PCs is complicated. The discrimination problem is related to the spectral similarity of different samples taken from the patient 194. The similarity of the tumor and normal sample from patient 194 may be explained by the fat content of both specimens. The tumor sample of 194 had a bright golden yellow color due to intracellular lipid accumulation. Normal sample 194 might be a cut of the adipose capsule of the kidney (or perinephric fat) which is a structure between the renal fascia and renal capsule. Nevertheless, in spite of the very strong measurement variance in the tumor samples in the PCA-space, the general trend is very promising and illustrates advantages of the multivariate (multi-channel) approach compared to a univariate sensing. None of the individual channels in Fig. 4 is capable of providing a similar degree of discrimination.

The class separation is much worse for the data set B. Again, the problem seems to be caused by unusual (compared to other) optical properties of several individual samples. Thus, tumor sample *T151* forms a very compact group of measurements at the left side of PC1, although the tumor is generally associated with a positive direction of PC1. This unusual appearance might be caused by the strong inhomogeneity of this tumor sample. In the highly heterogeneous layer there were a lot of necrotic regions, cystic changes, blood particles and some fat areas present (see Fig. 2, left). Measurement of each of these areas has led to a huge signal diversification. Some other inconsistencies correspond to specific positions on the sample. The measurements of the point *Cn* on the tumor sample *T144* are in the same way

randomly scattered, as the measured values of the whole tumor sample *T151*. On the contrary, *Cn* points of the normal sample *N144* of the same patient are typical “false positive” outliers (considering cancer as a “positive” test result). Elimination of the above sample and measurement positions only (they take about 18% of the whole data) significantly improves the separation statistics of PLS-DA analysis below.

Multivariate discrimination models have been built using PLS-DA algorithm. The latent variable space built by the PLS decomposition takes into account histological assignment of the samples to a “tumor” or “normal” class, i.e. the factor space is optimized for a particular discrimination task. For this reason PLS-DA is more effective for practical discrimination than PCA-based classification methods. PLS-DA calibration and cross-validation statistics for data sets A and B are presented in Table 1. Although the data set B exhibits worse discrimination, the presented statistical values of Sensitivity, Specificity and Accuracy indicate general practicability of tumor sensing using LED-based near infrared devices. Considering larger size and diversity of data set B, it better represents the real-life variability of the kidney tissue by oncology patients. Therefore, the data are not optimal for direct performance comparison of the two sensor models.

Table 1. PLS-DA statistics of cancer detection in data sets A and B.

| Data set          | nLV <sup>a</sup> | Calibration     |                 |                 |                 |                  |                  |                  | Cross-validation |                 |                 |                 |                  |                  |                  |
|-------------------|------------------|-----------------|-----------------|-----------------|-----------------|------------------|------------------|------------------|------------------|-----------------|-----------------|-----------------|------------------|------------------|------------------|
|                   |                  | TP <sup>b</sup> | FP <sup>c</sup> | TN <sup>d</sup> | FN <sup>e</sup> | Sns <sup>f</sup> | Spc <sup>g</sup> | Acc <sup>h</sup> | TP <sup>b</sup>  | FP <sup>c</sup> | TN <sup>d</sup> | FN <sup>e</sup> | Sns <sup>f</sup> | Spc <sup>g</sup> | Acc <sup>h</sup> |
| A33 <sup>i</sup>  | 2                | 19              | 1               | 11              | 2               | 91%              | 92%              | 91%              | 18               | 1               | 11              | 3               | 86%              | 92%              | 88%              |
| B170 <sup>j</sup> | 2                | 62              | 5               | 70              | 33              | 65%              | 93%              | 78%              | 59               | 7               | 68              | 36              | 64%              | 92%              | 75%              |
| B140 <sup>k</sup> | 2                | 64              | 3               | 67              | 6               | 91%              | 96%              | 94%              | 63               | 3               | 67              | 7               | 90%              | 96%              | 93%              |

<sup>a</sup> the number of latent variables in PLS-DA model; <sup>b</sup> True Positive; <sup>c</sup> False Positive; <sup>d</sup> True Negative; <sup>e</sup> False Negative;

<sup>f</sup> Sensitivity = TP/(TP+FN); <sup>g</sup> Specificity = TN/(FP+TN); <sup>h</sup> Accuracy = (TP+TN)/Total; <sup>i</sup> full data set A; <sup>j</sup> full data set B;

<sup>k</sup> data set B without sample *T151* and positions *N144\_Cn* and *T144\_Cn*

Relatively good reproducibility of measurements within individual samples and sample sites (*Cn* for the outliers) is an evidence of the technical quality of the method. Poor separation of classes in the case of the data set and sensor B is caused by the complexity of the data that could not be adequately captured by the four-channel device.

LEDs have been already successfully applied in miniaturized sensing devices in chemical sensing and optical diagnostics (e.g. the well-known pulse oximetry). The simplicity of use and low power consumption makes LEDs in combination with PDA (Photodiode Array) detectors a much more attractive option than tungsten-halogen lamps in optical/spectroscopic sensing devices. The miniaturization of diagnostic instruments is a very popular strategy in the development of medical devices. There is an increasing demand and a need to create small, handheld diagnostic sensors for in situ monitoring of vitality functions in real time. Typically, such devices (e.g. for monitoring of heart activity, oxygen or glucose level in the veins) are permanently implanted (or at least until they are replaced) and connected to a readout interface from which sensor data can be read out. A wireless transponder circuit of a sensing device, which is attached or brought into contact with tissue, makes the application even more attractive for surgical or histopathological practice. The LEDs based sensor to distinguish between tumor and nontumor tissue is a relatively new application, which is currently at the early development stage. In this paper, an experimental proof-of-concept demonstration of the LEDs based sensor for tumor differentiation using 4 wavelengths in NIR range has been presented. A wide spectrum of examinations of various organs and selection of suitable, relevant wavelengths needs to be performed in the development of the next prototype. Even if hitherto delivered results are widely scattered and their in-depth analysis does not achieve desired precision, nevertheless the perspectives are very promising.

The main disadvantage of the sensor in its present configuration is low Sensitivity caused by the very high variance of the measurements on cancer samples (Fig. 4). The tendency to give out false negatives is particularly dangerous in medical diagnostics; in oncology, they should be practically excluded. Therefore, improvement of the general Accuracy and tumor detection Specificity is the main requirement to further improvement of the sensor.

The sensor improvement can be achieved by further optimization of the number of channels and their working wavelengths. In optical technologies, the discrimination success basically relies on the sensor capability to recognize disease markers

by their spectral features. The most informative wavelengths should be found out based on a preliminary full-spectrum study of a representative sample set. Data quality can also be improved by the optimization of measurement parameters, including distance, angle, light intensity, and by using an appropriate reference. The probe construction can also be adapted to avoid various environmental effects, such as excessive water (contact measurement), surface highlights and ambient light. The above mentioned improvements are an important part of the future project work.

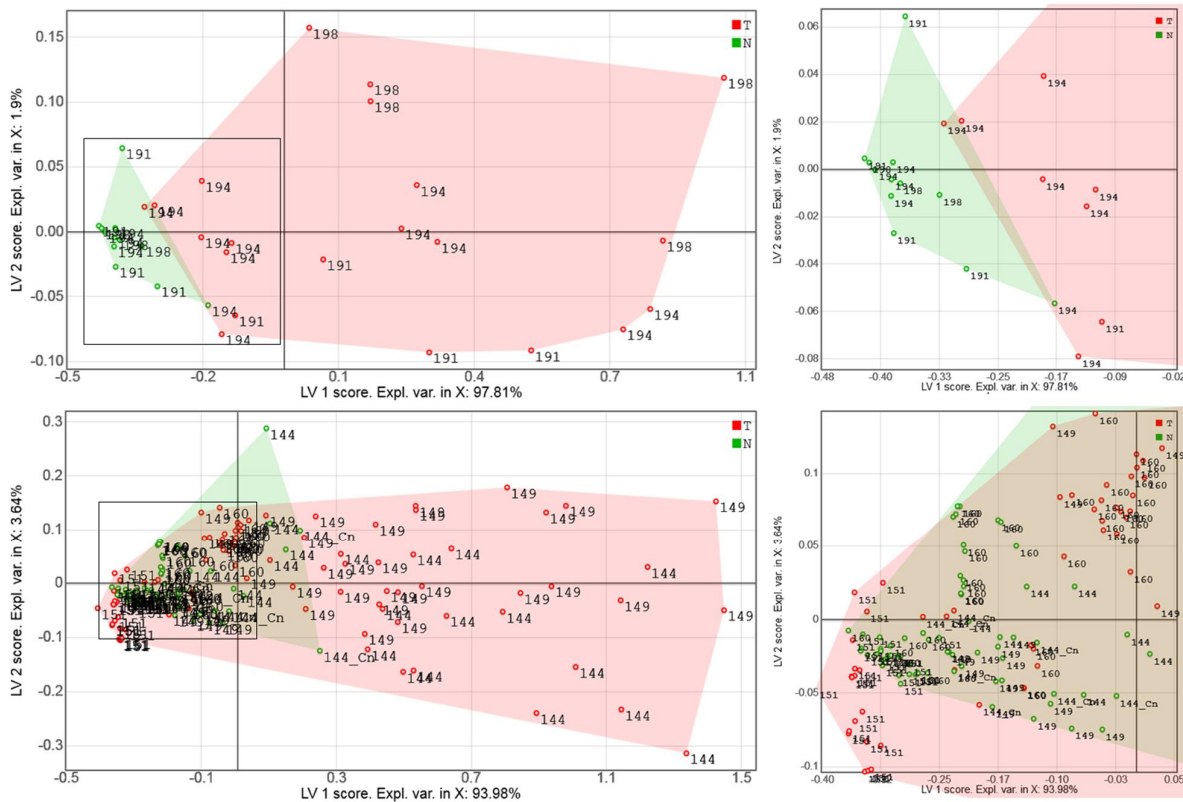


Fig. 5. LV1-LV2 scores for a PCA model on data sets A (top) and B (bottom), respectively. Zoom regions (areas inside rectangles) are shown magnified to the right of the main plots.

### Acknowledgement

Funding of the project by the European Union and European Regional Development Fund (Grant 10155837) is gratefully acknowledged. This work was supported by the Russian Ministry of Education and Science, within the framework of the basic part of state task on the theme: "Optical sensor technologies for quantitative and qualitative analysis in the industry and private life" (Project No. 3835). DK thanks DAAD for financial support of his research stay in Berlin (award # 50015559)

## REFERENCES

- [1] Artyushenko, V., Schulte, F., Zabarylo, U., Berlien, H.-P., Usenov, I., Saeb Gilani, T., Eichler, H., Pieszczek, Ł., Bogomolov, A., Krause, H., Minet, O., "Spectral fiber sensors for cancer diagnostics in vitro," Proc. SPIE 9537, Clinical and Biomedical Spectroscopy and Imaging IV, 953720 (July 15, 2015).
- [2] Nachabe, R., Hendriks, B. H., Schierling, R., Hales, J., Racadio, J. M., Rottenberg, S., Ruers, T. J., Babic, D. and Racadio, J. M., "Real-time in vivo characterization of primary liver tumors with diffuse optical spectroscopy during percutaneous needle interventions: feasibility study in woodchucks," Invest Radiol. 50(7), 443-448 (2015).
- [3] Nachabé, R., Evers, D. J., Hendriks, B. H., Lucassen, G. W., van der Voort, M., Wesseling, J. and Ruers, T. J., "Effect of bile absorption coefficients on the estimation of liver tissue optical properties and related implications in discriminating healthy and tumorous samples," Biomed. Opt. Express 2(3), 600–614 (2011).
- [4] Volynskaya, Z., Haka, A. S., Bechtel, K. L., Fitzmaurice, M., Shenk, R., Wang, N., Nazemi, J., Dasari, R. R. and Feld, M. S., "Diagnosing breast cancer using diffuse reflectance spectroscopy and intrinsic fluorescence spectroscopy," J. Biomed. Opt. 13(2), 024012 (2008).
- [5] Zhu, C., Breslin, T. M., Harter, J. and Ramanujam N., "Model based and empirical spectral analysis for the diagnosis of breast cancer," Opt. Express 16(19), 14961–14978 (2008).
- [6] Zhang, Y., Chen, Y., Yu, Y., Xue, X., Tuchin, V. V. and Zhu, D., "Visible and near-infrared spectroscopy for distinguishing malignant tumor tissue from benign tumor and normal breast tissues in vitro," J. Biomed. Opt. 18(7), 077003 (2013).
- [7] Cerussi, A., Shah, N., Hsiang, D., Durkin, A., Butler, J. and Tromberg, B.J., "In vivo absorption, scattering, and physiologic properties of 58 malignant breast tumors determined by broadband diffuse optical spectroscopy," J. Biomed. Opt. 11(4), 044005 (2006).
- [8] Chang, V. T.-C., Bean, S. M., Cartwright, P. S. and Ramanujam, N., "Visible light optical spectroscopy is sensitive to neovascularization in the dysplastic cervix," J. Biomed. Opt. 15(5), 057006 (2010).
- [9] Subhash, N., Mallia, J. R., Thomas, S. S., Mathews, A., Sebastian, P. and Madhavan J., "Oral cancer detection using diffuse reflectance spectral ratio R540/R575 of oxygenated hemoglobin bands," J. Biomed. Opt. 11(1), 014018 (2006).
- [10] Mallia, R. J., Narayanan, S., Madhavan, J., Sebastian, P., Kumar, R., Mathews, A., Thomas, G. and Radhakrishnan, J., "Diffuse reflection spectroscopy: an alternative to autofluorescence spectroscopy in tongue cancer detection," Appl. Spectrosc. 64(4), 409-418 (2010).
- [11] Amelink, A., Kaspers, O. P., Sterenborg, H. J., van der Wal, J. E., Roodenburg, J. L. and Witjes, M. J., "Non-invasive measurement of the morphology and physiology of oral mucosa by use of optical spectroscopy," Oral Oncol. 44(1), 65-71 (2008).
- [12] Kim, S. B., Temiyasathit, C., Bensalah, K., Tuncel, A., Cadeddu, J., Kabbani, W. and Liu, H., "An effective classification procedure for diagnosis of prostate cancer in near infrared spectra" Expert Systems with Applications 37(5), 3863-3869 (2010).
- [13] Sharma, V., Olweny, E., Kapur, P., Cadeddu, J., Roehrborn, C., and Liu, H., "Prostate cancer detection using combined auto-fluorescence and light reflectance spectroscopy: ex vivo study of human prostates," Biomed. Opt. Express 5(5), 1512-1529 (2014).
- [14] Sun, X., Xu, Y., Wu, J., Zhang, Y., and Sun, K., "Detection of lung cancer tissue by attenuated total reflection-Fourier transform infrared spectroscopy — a pilot study of 60 samples," J. Surg. Res. 179(1), 33-38 (2013).
- [15] Yi, W.-S., Cui, D.-S., Li, Z., Wu, L.-L., Shen, A.-G., and Hu, J.-M., "Gastric cancer differentiation using Fourier transform near-infrared spectroscopy with unsupervised pattern recognition," Spectrochim. Acta A Mol. Biomol. Spectrosc. 101, 127–131 (2013).
- [16] Maziak, D. E., Do, M. T., Shamji, F. M., Sundaresan, S. R., Perkins, D. G., and Wong, P. T. T., "Fourier-transform infrared spectroscopic study of characteristic molecular structure in cancer cells of esophagus: an exploratory study," Cancer Detect. Prev. 31(3), 244–253 (2007).
- [17] Eichler, J., Knot, J., and Lenz, H., "Measurements on the depth of penetration of light (0.35-1.0  $\mu\text{m}$ ) in tissue," Rad. Environm. Biophys. 14, 239-242 (1977).
- [18] Svaasand, L., "On the Physical Rationale of Photodynamic Therapy," editor – Gomer, C. J., [Future Directions and Application in Photodynamic Therapy], SPIE Institute Series for Advanced Optical Technologies, 233-248 (1990).

- [19] Galyanin, V., Melenteva, A. and Bogomolov, A., "Selecting optimal wavelength intervals for an optical sensor: A case study of milk fat and total protein analysis in the region 400–1100 nm," *Sensor. Actuat. B-Chem.* 218, 97–104 (2015).
- [20] Melenteva, A., Galyanin, V., Savenkova, E. and Bogomolov, A., "Building global models for fat and total protein content in raw milk based on historical spectroscopic data in the visible and short-wave near infrared range," *Food Chem.* 203, 190–198 (2016).
- [21] Qi, S., Ouyang, Q., Chen, Q. and Zhao, J., "Real-time monitoring of total polyphenols content in tea using a developed optical sensors system," *J. Pharm. Biomed. Anal.* 97, 116–122 (2014).
- [22] De Lima, K.M.G., "A portable photometer based on LED for the determination of aromatic hydrocarbons in water," *Microchem. J.* 103, 62–67 (2012).
- [23] Fuhrman, S. A., Lasky, L. C. and Limas, C., "Prognostic significance of morphologic parameters in renal cell carcinoma," *Am. J. Surg. Pathol.* 6(7), 655-663 (1982).
- [24] Moch, H., Artibani, W., Delahunt, B., Ficarra, V., Knuechel, R., Montorsi, F., Patard, J. J., Stief, C. G., Sulser, T. and Wild, P. J., "Reassessing the current UICC/AJCC TNM staging for renal cell carcinoma," *Eur. Urol.* 56(4), 636-643 (2009).
- [25] Fuhrman, S. A., Lasky, L. C., Limas, C., "Prognostic significance of morphologic parameters in renal cell carcinoma," *Am. J. Surg. Pathol.* 6(7), 655-663 (1982).
- [26] Nachabé, R., Evers, D. J., Hendriks, B. H. W., Lucassen, G. W., van der Voort, M., Rutgers, E. J., Vrancken Peeters, M. J., Van der Hage, J. A., Oldenburg, H. S., Wesseling, J., Ruers T. J. M., "Diagnosis of breast cancer using diffuse optical spectroscopy from 500 to 1600 nm: comparison of classification methods," *J. Biomed. Opt.* 16(8), 087010 (2011).
- [27] de Boer, L. L., Molenkamp, B. G., Bydlon, T. M., Hendriks, B. H., Wesseling, J., Sterenborg, H. J. and Ruers, T. J. M., "Fat/water ratios measured with diffuse reflectance spectroscopy to detect breast tumor boundaries," *Breast Cancer Res. Treat.* 152(3), 509-18 (2015).
- [28] Shah, N., Cerussi, A. E., Jakubowski, D., Hsiang, D., Butler, J. and Tromberg, B. J., "The role of diffuse optical spectroscopy in the clinical management of breast cancer," *Dis. Markers* 19(2, 3), 95-105 (2003, 2004).
- [29] Wold, S., Esbensen, K. and Geladi, P., "Principal component analysis," *Chemom. Intell. Lab. Syst.* 2, 37-52 (1987).
- [30] Brereton, R. G., [Chemometrics for Pattern Recognition], John Wiley & Sons, Ltd., Bristol, 199-200 (2009).
- [31] Drezek, R., Dunn, A. and Richards-Kortum, R., "A pulsed finite-difference time-domain (FDTD) method for calculating light scattering from biological cells over broad wavelength ranges," *Opt. Express* 6(7), 147–156 (2000).
- [32] Roth, W., Macher-Goeppinger, S. and Schirmacher, P., "Pathology and molecular pathogenesis of renal cell carcinoma," *Nephrologie* 6, 315-322 (2011).